

Dust Temperatures in the Infrared Space Observatory¹ Atlas of Bright Spiral Galaxies

George J. Bendo,^{2,3,4} Robert D. Joseph,³ Martyn Wells,⁵ Pascal Gallais,⁶ Martin Haas,⁷ Ana M. Heras,^{8,9} Ulrich Klaas,⁷ René J. Laureijs,^{8,9} Kieron Leech,^{9,10} Dietrich Lemke,⁷ Leo Metcalfe,⁸ Michael Rowan-Robinson,¹¹ Bernhard Schulz,^{9,12} and Charles Telesco¹³

ABSTRACT

We examine far-infrared and submillimeter spectral energy distributions for galaxies in the Infrared Space Observatory Atlas of Bright Spiral Galaxies. For the 71 galaxies where we had complete 60 - 180 μm data, we fit blackbodies with λ^{-1} emissivities and average temperatures of 31 K or λ^{-2} emissivities and average temperatures of 22 K. Except for high temperatures determined in some early-type galaxies, the temperatures show no dependence on any galaxy characteristic. For the 60 - 850 μm range in eight galaxies, we fit blackbodies with λ^{-1} , λ^{-2} , and $\lambda^{-\beta}$ (with β variable) emissivities to the data. The best results were with the $\lambda^{-\beta}$ emissivities, where the temperatures were ~ 30 K and the emissivity coefficient β ranged from 0.9 to 1.9. These results produced gas to dust ratios that ranged from 150 to 580, which were consistent with the ratio for the Milky Way and which exhibited relatively little dispersion compared to fits with fixed emissivities.

Subject headings: galaxies: ISM — galaxies: spiral — dust

1. Introduction

The far-infrared emission from galaxies is emitted by interstellar dust heated by a variety of energy sources. Two important energy sources are the general interstellar radiation field and the more intense radiation in star formation regions. These should produce dust sources at different dust temperatures and with different spatial distributions. Understanding these dust temperature components is necessary for understanding the relation between far-infrared emission and star formation in galaxies.

While much of the research in this subject has focused on ultraluminous galaxies and high redshift objects, some studies have investigated dust temperatures in normal spiral galaxies. However, no clear consensus has been reached on the temperatures of the dust components in spiral galaxies. Perhaps the most contentious issue is whether a significant dust component at a very low temperature ~ 10 -15 K exists. This issue needs to be resolved to understand how the interstellar radiation field and star formation regions heat dust to produce far-infrared emission.

Before the launch of the Infrared Space Observatory (ISO) (Kessler et al. 1996), most research on dust temperatures in galaxies relied on combining IRAS or Kuiper Airborne Observatory (KAO) data with ground-based submillimeter or millimeter data. The launch of ISO has permitted better far-infrared spectral energy distributions to be measured.

²Steward Observatory, 933 North Cherry Ave, Tucson, AZ 85721 USA; gbedo@as.arizona.edu

³University of Hawaii, Institute for Astronomy, 2680 Woodlawn Drive, Honolulu, HI 96822, USA; joseph@ifa.hawaii.edu

⁴Guest User, Canadian Astronomy Data Center, which is operated by the Dominion Astrophysical Observatory for the National Research Council of Canada's Herzberg Institute of Astrophysics.

⁵UK Astronomy Technology Center, Royal Observatory Edinburgh, Blackford Hill, Edinburgh EH9 3HJ, Scotland, UK; mw@roe.ac.uk

⁶CEA/DSM/DAPNIA Service d'Astrophysique, F-91191 Gif-sur-Yvette, France; gallais@discovery.saclay.cea.fr

⁷Max-Planck-Institut für Astronomie, Königstuhl 17, D-69117, Heidelberg, Germany; haas@mpia-hd.mpg.de, klaas@mpia-hd.mpg.de, lemke@mpia-hd.mpg.de

⁸Astrophysics Division, Space Science Department of ESA, ESTEC, P.O. Box 299, 2200 AG Noordwijk, Netherlands; aheras@ests2.estec.esa.nl, rlaureij@rssd.esa.int

⁹ISO Data Center, Astrophysics Division, ESA, Villafranca del Castillo, 28080 Madrid, Spain; lmetcalf@iso.vilspa.esa.es

¹⁰Saïd Business School, Park End Street, Oxford OX1 1HP, England, UK; kieron.leech@saïd-business-school.oxford.ac.uk

¹¹Astrophysics Group, Imperial College, Blackett Laboratory, Prince Consort Road, London SW7 2BZ, England, UK; m.rrobinson@ic.ac.uk

¹²IPAC, California Institute of Technology 100-22, Pasadena, CA 91125 USA; bschulz@ipac.caltech.edu

¹³Department of Astronomy, University of Florida, P.O. Box 112055, Gainesville, Florida 32611, USA; telesco@astro.ufl.edu

¹Based on observations with ISO, an ESA project with instruments funded by ESA Member States (especially the PI countries: France, Germany, the Netherlands and the United Kingdom) and with the participation of ISAS and NASA.

Smith (1982) was the first to measure a dust temperature in a non-active spiral. Using KAO data, he found a temperature of 20 K in NGC 5194 (M 51). Chini et al. (1986) combined submillimeter bolometer data from the NASA IRTF with IRAS far-infrared data to conclude that spiral galaxies have cold dust components with an average temperature of 16 K. Stark et al. (1989) measured far-infrared fluxes with the KAO and submillimeter fluxes with the NASA IRTF for three Virgo cluster spirals and inferred significantly warmer dust temperatures than those determined by Chini et al. (1986). Eales, Wynn-Williams, & Duncan (1989) measured dust temperatures in 11 galaxies using IRAS far-infrared data and submillimeter bolometer data from UKIRT and determined that the coolest dust component in spiral galaxies was 30 - 50 K, much warmer than previous measurements. These studies thus established a controversy over the apparently simple issue of the dust temperatures in spiral galaxies.

Subsequent studies have produced similarly conflicting results. Most have focused on individual galaxies, including NGC 660, UGC 3490 (Chini & Krügel 1993), NGC 3267 (Sievers et al. 1994), NGC 4631 (Braine et al. 1995), M 51 (Guèlin et al. 1995; Hippelein et al. 1996), M 101 (Hippelein et al. 1996), the Andromeda Galaxy (Haas et al. 1998), and NGC 891 (Popescu et al. 2000). These studies typically find dust temperatures of ~ 20 K, with the lowest temperature being 16 K and the highest being 33 K. There have been a few studies of larger samples. Some of these surveys have found far-infrared dust temperatures as high as 35 K (Clements, Andreani, & Chase 1993; Dunne et al. 2000). Others have found temperatures between 20 and 30 K (Dunne & Eales (2001); Popescu et al. (2002)), and still others have found dust components as cold as 10-15 K (Chini et al. 1995; Krügel et al. 1998; Siebenmorgen, Krügel, & Chini 1999; Stickel et al. 2000).

Part of the reason no consensus has been reached on dust temperatures in normal galaxies is because of poor sampling of the spectral energy distribution (SED). To find reliable dust temperatures it is vital to evenly sample the SEDs from the Wien side to the Rayleigh-Jeans side of the Planck spectrum. Some studies have had such poor spectral sampling that Planck functions are fit to data with no degrees of freedom, and some have entire dust temperature components defined by a single measurement. Another source of the discrepancy is that different studies assume different wavelength dependences for the emissivity. In general when a shallower emissivity function is chosen, this produces warmer temperatures.

In this paper we combine far-infrared ISO photometry with submillimeter photometry from the Submillimetre Common-User Bolometer Array (SCUBA) (Holland et al. 1999) at the James Clerk Maxwell Telescope (JCMT) to sample the full spectrum of cool dust emission in normal spiral galaxies. We will first present the dust temper-

atures we infer from 60, 100, and 180 μm ISO measurements for 71 spiral galaxies in the ISO Atlas of Bright Spiral Galaxies (Bendo et al. 2002) (henceforth referred to as Paper 1). We then examine dust temperatures obtained by combining the far-infrared data with submillimeter data for 8 of the galaxies in the sample. Finally, we calculate dust masses and examine gas to dust mass ratios for 7 of these galaxies.

2. Data

2.1. The Sample

The galaxies in this sample are a subset of a complete, magnitude-limited set of galaxies selected from the Revised Shapley-Ames (RSA) Catalog (Sandage & Tammann 1987). The sample comprised galaxies with Hubble types between S0 and Sd and with magnitudes $B_T = 12$ or brighter; galaxies in the Virgo Cluster were excluded. A randomly selected, subset of these galaxies was observed by ISO based on target visibility. This produced a total of 77 galaxies that are representative of the range of Hubble types in the RSA Catalog, 71 of which were observed successfully with ISOPHOT. Detailed information on the sample is presented in Paper 1.

2.2. Observations and Data Analysis

2.2.1. Far-Infrared Photometry

The 60, 100, and 180 μm photometric data were taken with ISOPHOT (Lemke et al. 1996) and processed with PIA 8.0 (Gabriel et al. 1997) with additional processing to correct for PSF effects, as discussed in Paper 1. Note that, for the analysis without the submillimeter data, we assume that the 180 μm flux within the 180 arcsec apertures effectively comes from the same sources as the 60 and 100 μm fluxes within a 135 arcsec aperture. To investigate how much extra far-infrared flux may come from the region outside the 135 arcsec aperture but within the 180 arcsec aperture, we investigated the distribution of infrared flux in maps of IRAS data made by the HIRES software package provided by the Infrared Processing and Analysis Center. We find that the median ratio of flux within 135 arcsec to flux within 180 arcsec is 0.85 at 60 μm and 0.80 at 100 μm for the galaxies in this sample. According to the HIRES beam profiles, point sources would have ratios of 0.95 at 60 μm and 0.85 at 100 μm . The small difference between the ratio of fluxes for the sample galaxies and the ratio expected for point sources suggests that most of the emission between the 135 and 180 arcsec apertures in the HIRES maps is mostly from the point spread function and that emission in those regions is relatively small in most galaxies. We will assume that the distribution of the 180 μm emission will be similar to the 100 μm emission, so therefore, we will assert that most of the 180 μm emission for the galaxies in this sample also comes from within 135 arcsec. When we also

have submillimeter data, however, we can make assumptions about the spatial distribution of the emission and perform a deconvolution analysis to estimate the 180 μm fluxes within 45 and 135 arcsec apertures.

2.2.2. Submillimeter Photometry

We observed NGC 4088 and NGC 4826 at 850 μm using SCUBA at the JCMT. The data were taken in jiggle map mode, in which the telescope's secondary mirror shifts in a 64-point pattern to create a completely sampled map for the inner 135 arcsec of the target. For sky subtraction, we nodded 2 arcmin off-source parallel to the optical disks' minor axes for each galaxy. Integration times were 64 min for NGC 4088 and 60 min for NGC 4826. We performed skydips regularly to check the opacity during the observations. At 850 μm , the opacity typically ranged between 0.3 and 0.6 for all the observations. (The high sky opacity made the simultaneous 450 μm observations useless.) For calibration, we observed Mars using similar methods.

In addition to the above data, we have used data from the JCMT SCUBA archives for 6 galaxies: NGC 4414, NGC 4631, NGC 5236, NGC 5713, NGC 5792, and NGC 5907. All of these data were taken in SCUBA's jiggle map mode, with either Uranus, OH 231.8, or IRC +10216 used for calibration.

The data were processed with the SCUBA User Reduction Facility (Jenness & Lightfoot 1998) following the typical processing steps. First, the data were flat-fielded and corrected for airmass and sky opacity. Bad bolometers were flagged and masked. An additional background selection was made by measuring and subtracting surface brightnesses in selected off-target bolometers using the "remsky" procedure. Finally, the data were combined together and rebinned to produce final maps. Images of planets and other calibration sources were processed using the same methods. Signals were measured within 45 and 135 arcsec apertures, which are comparable to the apertures of ISOPHOT. For calibration, we measured the signals from the standard sources in similarly-sized apertures, and these then provided conversion factors for converting signals to flux densities for the targets. We assume that the uncertainty in both the new measurements and the archival measurements comes primarily from the uncertainty in the calibration, which is approximately 10 %. Other sources of uncertainty, mainly uncertainties from background noise, appear to be less significant. Table 1 lists the resulting flux densities as well as the optical diameter parameter from the Third Reference Catalogue of Bright Galaxies (de Vaucouleurs et al. 1991) and an indication of whether the data came from original observations or the JCMT SCUBA archives.

3. Spectral Energy Distributions and Dust Temperatures

3.1. Far-Infrared Spectral Energy Distributions

First, we fit blackbody functions with two different emissivity functions to the data. The emissivity functions we selected scale as λ^{-1} and λ^{-2} , functions that are used by many studies cited in Section 1 and that are recommended by Hildebrand (1983).

Table 2 lists the dust temperatures determined from the ISO far-infrared data, and Figure 1 shows histograms of these temperatures. We estimate an error of ~ 2 K in the dust temperatures due to uncertainties in the photometric calibration of ISOPHOT. This error was determined by fitting blackbodies to data where the 60 μm flux was increased 20 % and the 180 μm flux was decreased 20 % and vice-versa. The temperatures of the fits are, for the λ^{-1} emissivity, a mean of 31 K with a range of 24 - 42 K, and, for the λ^{-2} emissivity, a mean of 25 K with a range of 21 - 32 K. The functions with the λ^{-1} emissivities generally fit the data better according to the χ^2 criterion.

The dust temperatures vary little in relation to morphology and AGN activity. The data in Table 3 do show that some S0 and elliptical galaxies tend to have warmer dust temperatures, but all the spiral and irregular galaxies have indistinguishable dust temperatures.

These results should be compared with those of Stickel et al. (2000), who used IRAS 60 and 100 μm data supplemented by 170 μm photometry from the ISO Serendipity Survey for 115 galaxies. They assumed an emissivity function scaling as λ^{-2} and found a temperature distribution centered at 20 K with a range of 15-25K. These results are systematically colder by 5-6 K and they conclude that "for the first time this indicates that a cold dust component with $T_D \leq 20$ K is present in a large fraction of all spiral galaxies." In contrast, using the same emissivity function we find no galaxy with $T_D < 21$ K and no support for such a cold dust component in most spiral galaxies. One possible explanation could be that Stickel et al. (2000) use IRAS Faint Source Catalog (FSC) data at 60 and 100 μm , whereas we have used ISO photometry at 60 and 100 μm and were able to make approximate corrections for the point spread function. As we demonstrated in Paper 1, the ISO fluxes used in this research, particularly the 60 μm fluxes, are systematically higher than those in the IRAS FSC Catalog, which would naturally lead to the temperatures found using the ISO photometry to be higher than those found using corresponding IRAS FSC data.

However, some qualifications must be made to interpretations based on data confined to this relatively small wavelength range, even though these data from ISO include the longer wavelength 180 μm measurement which IRAS did not have. First, if dust components 10-15 K ex-

ist, their contribution would not be evident using the far-infrared data alone. Second, emission at 60 μm may include emission from warmer dust components that cause the spectral energy distribution to flatten out (see Laureijs et al. (2000) for an example based on observational data of galactic cirrus, Popescu et al. (2000) and Dunne & Eales (2001) for examples of blackbody fits to observations of nearby galaxies, or Désert, Boulanger, & Puget (1990) and Dale et al. (2001) for detailed modeling of dust emission at far-infrared wavelengths). Thus, fitting single blackbody functions through the 60, 100, and 180 μm data points is possible but may not accurately describe the physics of the dust emission. The addition of longer wavelength data may provide evidence for more than one dust component. Therefore, in the next section, we examine the blackbody fits obtained when the far-infrared data are combined with submillimeter data.

3.2. Far-Infrared to Submillimeter Spectral Energy Distributions

We have submillimeter and far-infrared data for a subset of 8 of the ISO galaxy sample, and blackbody functions with λ^{-1} and $\lambda^{-\beta}$ emissivities, with β variable, have been fitted to these data. We refer to the resulting dust temperatures measured within 135 arcsec apertures as global dust temperatures. We also determined the temperatures of dust within the inner 45 arcsec of the galaxies, and we refer to these as the nuclear dust temperatures. (We note our designation "nuclear" is very qualitative; at the distances of these galaxies 45 arcsec subtends ≥ 1 kpc, a much larger region than would normally be considered the galaxy nucleus. Starburst regions in galaxies are typically 250 - 500 pc.) The dust temperatures measured within a 135 arcsec aperture but outside a 45 arcsec aperture we refer to as disk temperatures. These distinctions permit investigation of the differences between dust temperatures in the inner and outer regions of these galaxies.

Since the diffraction limit of the ISO telescope at 180 μm is ~ 145 arcsec, to do this analysis for the 180 μm data requires estimating the fluxes from both central unresolved and extended components. We use a method similar to that used by Radovich et al. (1999). (We also used this method for the 60 and 100 μm data in Paper 1.) We calculate the ratio of fluxes for the point and extended sources at both 100 μm and 850 μm , since we have the required 45 arcsec resolution at both these wavelengths. We then interpolate to estimate the ratio of the 180 μm fluxes from point and extended components. According to Laureijs (1999)¹⁴,

61.2 % of the flux from a point source centered in the C200 array (the 180 μm measurement) will fall on the array. Therefore the flux within the 180 arcsec aperture

can be expressed as

$$f_m(180'') = 0.612f_c + (180'')^2 f_e. \quad (1)$$

where f_m is the measured flux, f_c is the flux from the central source, and f_e is the flux per arcsec² from a diffuse, uniform, extended source. Substituting the ratio $\frac{f_c}{(180'')^2 f_e}$ into the above equation allows for solving for f_c and f_e :

$$f_c = \frac{f_m}{0.612 + \frac{(180'')^2 f_e}{f_c}} \quad (2)$$

$$f_e = \frac{f_m}{0.612 \frac{f_c}{(180'')^2 f_e} + 1} \quad (3)$$

These central and extended components can then be used to calculate fluxes within 45 and 135 arcsec apertures:

$$f_t(45'') = f_c + (45'')^2 f_e \quad (4)$$

$$f_t(135'') = f_c + (135'')^2 f_e. \quad (5)$$

The resulting 180 μm flux densities are listed in Table 4. We can now use these 180 μm flux estimates for the dust temperature analysis outlined above.

Table 5 lists the resulting dust temperatures derived using the λ^{-1} emissivities, and Table 6 lists the dust temperatures for $\lambda^{-\beta}$ emissivities. In addition, Figures 2 - 9 show the spectral energy distributions and the fits of blackbody functions with $\lambda^{-\beta}$ emissivities. We also tried fitting single blackbodies with λ^{-2} emissivities to the data, but except for NGC 5236 (which will be discussed below) the fits were very poor. We estimated an error of ~ 1 K in these dust temperatures using the same method described above for the far-infrared spectral energy distributions. In summary, the fits yield dust temperatures of ~ 35 K for models with λ^{-1} emissivities and ~ 30 K for models with $\lambda^{-\beta}$ emissivities. Typical fits to the emissivity coefficient were between 0.9 and 1.4.

NGC 5236 is exceptional in that the emissivity function is closer to λ^{-2} . NGC 5236 is a galaxy with unusual supernova activity. Shocks from the strong supernova activity associated with the galaxy's nucleus could be responsible for breaking up larger dust grains into smaller grains, thus making the wavelength dependence of the emissivity function steeper. The disk of NGC 4414, but not the nucleus, also exhibits a steep emissivity. Star formation has been inhibited in the nucleus by the lack of molecular gas present (Sakamoto 1996), but sites of strong star formation are evident in the disk (*cf.* Fig. 25 in Paper 1), and the large dust grains may have suffered similar fragmentation as in NGC 5236.

In general, the "nuclear" dust temperatures are systematically warmer than the disk temperatures in all cases. Because stellar densities are higher in the nuclei of these galaxies, and because the star formation rate may be higher, the interstellar radiation field is stronger. This

¹⁴http://www.iso.vilspa.esa.es/users/expl_lib/PHT/c200fpsf02.ps.gz

enhances both the dust emission and the dust temperatures, producing the observed differences in dust temperatures between the nuclear and disk regions.

Since some other studies have suggested there are two temperature components, we have also investigated the possibility that the dust emission may be composed of two blackbody components. This obviously requires steeper wavelength-dependence for the emissivities. We therefore chose emissivity functions proportional to λ^{-2} for both temperature components. Table 7 shows the best fitting temperatures, with two temperatures derived for all galaxies except NGC 5236. (For NGC 5236, the analysis demonstrates that a second blackbody component would make only a minor contribution to the far-infrared and submillimeter spectral energy distribution, so only one component was fit to the data.) In most cases, the two components have temperatures of ~ 15 K and ~ 30 K. For galaxies with no 450 μm data, the solution is an even-determined problem with an exact fit that should be interpreted with caution. Moreover, the colder dust temperature is dependent mainly on the submillimeter measurement, so errors in the submillimeter measurement directly affect the temperature of the coldest component.

Having used submillimeter data to determine dust temperatures for these 8 galaxies, we can now compare the temperatures found for these same galaxies used the ISO far-infrared data alone. Comparing the dust temperatures in Table 2 with the "Global" temperatures in Table 5 and Table 7 shows that the addition of the submillimeter data systematically increases the derived dust temperatures ~ 2 -3 K. The more significant difference is that, by adding the submillimeter data point(s) one can search for a very cold dust component of temperature ~ 6 -15 K.

In summary, for these 8 galaxies with both ISO far-infrared and submillimeter measurements, we find dust temperatures in almost all cases that can be described as a ~ 35 K blackbody with a λ^{-1} emissivity, a ~ 30 K blackbody with a variable emissivity coefficient ranging from 0.9 to 1.4, or two blackbodies with temperatures of ~ 15 K and ~ 30 K and λ^{-2} emissivities. Clearly the far-infrared-to-submillimeter spectral energy distributions of galaxies can be represented with several different functions and correspondingly larger or smaller dust temperatures. This is essentially a duplication of the variety of results found in the literature for the past two decades. The key question is, which of these is most likely to be correct? We return to this question in the Discussion.

4. Gas to Dust Mass Ratios

The accurate measurement of dust temperatures is not only necessary for understanding dust emission in galaxies. It is also required for measuring the gas to dust ratios in spiral galaxies. As discussed by Devereux &

Young (1990), the temperatures and dust masses measured with IRAS data, when combined with molecular gas data, produced gas to dust mass ratios of approximately 1000. This is a factor of 10 larger than the value for the Milky Way and it therefore raises a serious problem. This problem has also appeared in most other studies in which cold dust components have been found. The ISO Serendipity Survey by Stickel et al. (2000) is a notable exception; the typical gas-to-dust mass ratios found are near that of the Milky Way, but the ratios range from 50 to 1000. If these results are reliable they raise the question whether this basic property of the interstellar medium really varies so dramatically among galaxies.

Young et al. (1995) list CO flux measurements for the 8 galaxies for which we have far-infrared and submillimeter flux measurements. Using their data and their conversion of CO intensities to molecular gas surface densities, we calculated molecular gas densities. We then used the 850 μm flux densities and the dust temperatures and the associated emissivity assumptions used to fit the SEDs to calculate dust masses. Working at 850 μm is preferred because the determination of dust masses at that wavelength is relatively insensitive to uncertainties in dust temperatures. With these masses, we then calculated gas to dust ratios that may be compared to the Milky Way ratio.

4.1. Dust Masses and Gas to Dust Mass Ratios

We calculated dust masses using

$$M_{Dust} = \left[\frac{F(\nu)D^2}{B(\nu, T)} \right] \left[\frac{4a}{3Q(\nu)} \right] \rho \quad (6)$$

derived in Hildebrand (1983). M_d is the dust mass, $F(\nu)$ is the measured flux density, D is the distance, $B(\nu, T)$ is the flux density from a blackbody of temperature T , a is the approximate average size of an interstellar dust grain, $Q(\nu)$ is the emissivity, and ρ is the density of a dust grain. Since these are nearby spiral galaxies, we assume that these galaxies contain dust with properties similar to the dust in the Milky Way. Therefore, we have also used the assumptions in Hildebrand (1983) for calculating dust masses. The size and density of the dust grains are assumed to be $a = 0.1 \mu\text{m}$ and $\rho = 3 \text{ g cm}^{-3}$. For the emissivities, we use the expression

$$Q(\lambda, \beta) = Q_0 a \left(\frac{250}{\lambda} \right)^\beta \quad (7)$$

from Klaas et al. (2001), where $Q_0 = 40 \text{ cm}^{-1}$ and β is the emissivity coefficient. This equation gives $Q(850\mu\text{m}, 1) = 1.2 \times 10^{-4}$ and $Q(850\mu\text{m}, 2) = 3.5 \times 10^{-5}$.

Table 8 lists the global dust masses calculated from the data in Tables 1, 5, 6, and 7. Dust masses calculated with steeper emissivity laws are always higher than those calculated with shallower emissivity laws for two

reasons. First, the fits to the spectral energy distribution using the shallower emissivity function produce higher temperatures than those fits using the steeper emissivity functions. These higher temperatures lead to higher values of $B(\nu, T)$, which then result in lower calculated dust masses. The second is the difference in the dust grain emissivity values at $850 \mu\text{m}$. The emissivity is higher for shallower emissivity functions, which leads to lower calculated dust masses. Essentially, a higher temperature or a higher emissivity requires less dust to produce the measured submillimeter flux.

Table 8 also presents global molecular gas masses calculated from the data in Young et al. (1995) and the resulting global gas to dust mass ratios. (We did examine gas to dust ratios for separate nuclear and disk regions, but the comparison showed no clear distinction between nuclear and disk ratios.)

4.2. Discussion

Inspection of Table 8 shows that the gas to dust ratios ultimately depend on the emissivity function used to fit the data. Perhaps even more importantly, when the emissivity coefficient is fixed (i.e. proportional to λ^{-1} or λ^{-2}), the range of gas to dust ratios for these 8 galaxies varies by factors of 20 - 30. With the λ^{-1} emissivities, the ratios range from 130 to 2700, and with the λ^{-2} emissivities and two temperature components, the ratios range from 13 to 480. However, when the emissivity coefficient is fit to the data, the gas to dust ratios vary from 150 to 580, only a factor ~ 4 .

We may check the plausibility of these calculated gas to dust ratios using the Milky Way ratio as a benchmark. The molecular gas to dust ratio in the Milky Way has been determined to be 115 using COBE data (Sodroski et al. 1994). The median gas to dust ratio for the λ^{-1} emissivity fits is approximately a factor of 6 higher than the ratio for the Milky Way, so the single blackbody with the λ^{-1} emissivity is unlikely to accurately represent the physical conditions of the dust. The median ratio from the λ^{-2} emissivity fit is within a factor of 3 of the Milky Way value, so these fits are more plausible. The median ratio from the $\lambda^{-\beta}$ emissivity fits is also within a factor of 3, so these fits are equally plausible. Dale & Helou (2002), however, have demonstrated empirically that fitting one or two blackbodies to far-infrared and submillimeter data may lead to underestimates of the dust mass by as much as a factor of 10 when compared to more realistic models that fit a series of blackbodies to the data. If we accept that this effect is present, the λ^{-1} and $\lambda^{-\beta}$ emissivity fits would produce gas to dust ratios near the Milky Way's but the λ^{-2} emissivity ratios would be much too low to be plausible.

However, the range in ratios provides an additional criterion for comparing the three fits. The dust masses computed using both the λ^{-1} emissivity and the two-

component model with very cold dust give gas-to-dust ratios which vary from galaxy to galaxy by factors of 20 and 37 respectively. In contrast, the range in the ratios for the $\lambda^{-\beta}$ fits is less than a factor of 4. Since these are all nearby spiral galaxies, we would expect the basic properties of the interstellar medium to be similar. If the best description of the dust is the one that gives the lowest dispersion in the gas-to-dust ratios, and gas/dust ratios which are similar to that for the Milky Way, then the $\lambda^{-\beta}$ emissivity fits are clearly preferred. The fits with the fixed emissivities give implausible variations in the gas-to-dust ratios, while the $\lambda^{-\beta}$ fits give a more acceptable range.

As a result, using both closeness to the Milky Way gas-to-dust ratio and the small dispersion of the ratios as an indication of the plausibility for the gas-to-dust ratios, it is evident that the fits using the $\lambda^{-\beta}$ emissivity, i.e. the right-hand column of Table 8, provide results that are most likely to be correct for the galaxies in this sample.

We are now able to address the larger question of the lack of consensus in the dust temperatures and even the number of different temperature components in normal galaxies which was described in the Introduction. It is clear from the analysis above that one can fit spectral energy distributions from $60 - 850 \mu\text{m}$ equally well by a) a single temperature component with emissivity proportional to λ^{-1} , b) a single temperature component with emissivity proportional to $\lambda^{-\beta}$, or c) two temperature components, one of which is "cold," with a temperature ~ 15 K, and the other with temperature ~ 30 K. This range of results is just what one finds in reviewing the literature on this subject over the past 20 years. We suggest it is the assumptions made about the emissivity function in different studies which have largely produced the wide range of conclusions about the dust temperatures and dust masses in galaxies and the lack of consensus which has plagued this subject. We have shown that that the assumptions most commonly used lead to implausible gas-to-dust ratios. The distinguishing feature of this study is that we have tested the physical plausibility of various possible emissivity functions rather than adhering rigidly to an assumed emissivity function and calculating dust temperatures and other parameters.

So, having shown that the $\lambda^{-\beta}$ emissivity fits to the spectral energy distributions imply more plausible dust masses and gas-to-dust ratios than the other choices, what is the physical interpretation of this result? First we note that in this model we use only one temperature component to approximate the dust emission when there is almost certainly a range of dust temperatures both within star formation regions and in the diffuse interstellar medium. Does this make sense? A priori, a two-component model might be more reasonable since a warmer component from star formation regions and a cooler component from dust heated by the diffuse interstellar radiation field are expected. Since such models

appear to result in dust masses that are too large and gas-to-dust ratios that are implausibly small, this suggests that the colder component in such models is a less significant contributor than the two-component fits imply. Since only a single temperature gives plausible dust masses, we suggest that if a second cold component to the dust emission from the diffuse interstellar medium is present, it is relatively insignificant in terms of both its contributions to the mass and to the SED. To distinguish its contribution apparently requires better spectral coverage and photometric precision in the submillimeter and millimeter regions than has been available heretofore.

We must also consider the physical interpretation of a variable emissivity law due to the varying β we find for this galaxy sample. The emissivity functions should be related to the average physical properties of the dust, such as the composition and grain size distribution, and these are expected to be relatively constant among nearby spiral galaxies. Is it not inconsistent to argue that the emissivity functions can vary when we also argue that the gas-to-dust ratios should be similar among spiral galaxies? We suggest two plausible interpretations for this result. First, it may be that the grain properties do vary among these galaxies. Dale & Helou (2002) and references therein present data that demonstrate how β may depend on environment. However, they argue that β should decrease as the temperature of dust increases, which is the opposite of the trend we have found. Instead, we suggest that galaxies which have undergone significant recent star formation activity and concomitant supernovae may have a somewhat altered dust grain population. Supernova shock waves can break down silicate grains with carbon mantles into individual silicate and graphite grains. Silicate grains have different emissivities than the graphite grains, so the average emissivity would change. Furthermore, the destruction of very large grains would make the emissivity function steeper. Breaking down the dust with supernova shock waves also suggests some dust grain destruction (Dyson & Williams 1997), which is exactly what is seen in these results for galaxies with steep emissivities. An alternative interpretation might be that the varying emissivity function is simply a second fitting parameter, in addition to a temperature, and this combination better accounts for the range of dust temperatures and other dust properties that are found in spiral galaxies.

5. Conclusions

We have shown that, for the 71 galaxies in the ISO Atlas sample, the 60 - 180 μm spectral energy distributions have mean temperatures of 31 K for the λ^{-1} emissivities and 25 K for the λ^{-2} emissivities. The blackbodies with λ^{-1} emissivities generally fit the data better than the ones with λ^{-2} emissivities. Analysis of the dust temperatures as a function of morphological type reveals that

spirals from Sa-Scd have remarkably uniform dust temperatures which are virtually identical within the errors. Dust temperatures are enhanced above the average for the spirals only in E/SO galaxies and in galaxies with especially strong star formation activity. Data based on SEDs over this spectral range do not support the existence of a substantial cold component at a temperature < 20 K in a large fraction of spiral galaxies, in contrast to some earlier studies.

For the eight galaxies in the sample with the spectral energy distributions measured from 60 - 850 μm , we showed that the 60 - 850 μm spectral energy distributions could be fit equally well by: a) a single temperature component with emissivity proportional to λ^{-1} , b) a single temperature component with emissivity proportional to $\lambda^{-\beta}$, or c) two temperature components, one of which is "cold," with a temperature ~ 15 K. We suggest that the enormous variation in reported dust temperatures and dust masses that characterize the literature on spiral galaxies is largely a reflection of the variety of assumptions for the emissivity functions employed.

To choose among these three assumptions we used the gas-to-dust ratio as a criterion. Only the temperatures derived using the single temperature component with emissivity proportional to $\lambda^{-\beta}$ produced gas-to-dust ratios within a rather narrow range and one that was close to the gas-to-dust ratio for the Milky Way. We suggest that these results are most likely to represent the actual dust properties of normal spiral galaxies. In particular, we find the wide range in inferred gas-to-dust ratios derived with the assumption of a "cold" dust component less physically plausible than those ratios derived using a single temperature component with temperatures derived using $\lambda^{-\beta}$, with β calculated for each galaxy.

G. J. B. would like to thank Iain Coulson and Loretta Dunne for their help with the submillimeter observations and data processing; Daniel A. Dale for his comments on this paper; and the staff of IRAS for providing the HIRES data.

The ISOPHOT data presented in this paper were reduced using PIA, which is a joint development by the ESA Astrophysics Division and the ISOPHOT Consortium with the collaboration of the Infrared Processing and Analysis Center (IPAC). Contributing ISOPHOT Consortium institutes are DIAS, RAL, AIP, MPIK, and MPIA.

The JCMT is operated by the Joint Astronomy Center on behalf of the UK Particle Physics and Astronomy Research Council, the Netherlands Organization for Scientific Research, and the Canadian National Research Council.

This research has been supported by NASA grants NAG 5-3370 and JPL 961566.

REFERENCES

- Bendo, G. J., et al. 2002, *AJ*, 123, 3067 (Paper 1)
- Braine, J., Krügel, E., Sievers, A., & Wielebinski, R. 1995, *A&A*, 295, L55
- Chini, R., Kreysa, E., Krügel, E., & Mezger, P. G. 1986, *A&A*, 166, L8
- Chini, R. & Krügel, E. 1993, *A&A*, 279, 385
- Chini, R., Krügel, E., Lemke, R., & Ward-Thompson, D. 1995, *A&A*, 295, 317
- Clements, D. L., Andreani, P., & Chase, S. T. 1993, *MNRAS*, 261, 299
- Dale, D. A., & Helou, G. 2002, preprint (astro-ph/0205085)
- Dale, D. A., Helou, G., Contursi, A., Silbermann, N. A., & Kolhatkar, S. 2001, *ApJ*, 549, 215
- Désert, F.-X., Boulanger, F., & Puget, J. L. 1990, *A&A*, 237, 215
- de Vaucouleurs, G., de Vaucouleurs, A., Corwin, H. G., Buta, R. J., Paturel, G., & Fouque, P. 1991, *Third Reference Catalogue of Bright Galaxies* (Berlin: Springer-Verlag)
- Devereux, N. A., & Young, J. S. 1990, *ApJ*, 359, 42
- Dunne, L., Eales, S., Edmunds, M., Ivison, R., Alexander, P., & Clements, D. L. 2000, *MNRAS*, 315, 115
- Dunne, L., & Eales, S. 2001, *MNRAS*, 327, 697
- Dyson, J. E., & Williams, D. A. 1997, *The Physics of the Interstellar Medium* (2d ed.; Bristol: Institute of Physics Pub)
- Eales, S. A., Wynn-Williams, C. G., & Duncan, W. D. 1989, *ApJ*, 339, 859
- Gabriel, C., et al. 1997, in *ASP Conf. Ser. 125, Astronomical Data Analysis Software and Systems (ADASS) VI*, ed. G. Hunt & H.E. Payne, (San Francisco: ASP), 108
- Guèlin, M., Zylka, R., Mezger, P. G., Haslam, C. G. T., & Kreysa, E. *A&A*, 298, L29
- Haas, M., Lemke, D., Stickel, M., Hippelein, H., Kunkel, M., Herbstmeier, U., & Mattila, K. 1998, *A&A*, 338, L33
- Hildebrand, R. H. 1983, *QJRAS*, 24, 267
- Hippelein, H., et al. 1996, *A&A*, 315, L82
- Holland, W. S., et al. 1999, *MNRAS*, 303, 659
- Jenness, T., & Lightfoot, J. F. 1998, in *Astronomical Data Analysis Software and Systems VII*, ed. R. Albrecht, R. N. Hook, & H. A. Bushouse (San Francisco: ASP), 216
- Kessler, M.F., et al. 1996, *A&A*, 315, L27
- Klaas, U., et al. 2001, *A&A*, 379, 823
- Krügel, E., Siebenmorgen, R. Zota, V., & Chini, R. 1998, *A&A*, 331, L9
- Laureijs, R. J. 1999, "Point Spread Function Fractions Related to the ISOPHOT C100 and C200 Arrays", Version 1.0 (Noordwijk: ESA)
- Laureijs, R. J., Herbstmeier, U., Ábrahám, P., Klaas, U., & Lemke, D. 2000, in *ISO Beyond Point Sources*, ed. R. J. Laureijs, K. Leech, & M. F. Kessler (Noordwijk: ESA Publications Division), 131
- Lemke, D., et al. 1996, *A&A*, 315, L64
- Popescu, C. C., Misiriotis, A., Kylafis, N. D., Tuffs, R. J., & Fishera, J. 2000, *A&A*, 362, 138
- Popescu, C. C., Tuffs, R. J., Völk, H. J., Pierini, D., & Madore, B. F. 2002, *ApJ*, 567, 221
- Radovich, M., Klaas, U., Acosta-Pulido, J., & Lemke, D. 1999, *A&A*, 348, 705
- Sakamoto, K. 1996, *ApJ*, 471, 173
- Sandage, A., & Tammann, G. A. 1987, *A Revised Shapley-Ames Catalog of Bright Galaxies 2nd ed.* (Washington: Carnegie Institution)
- Siebenmorgen, R., Krügel, E., & Chini, R. 1999, *A&A*, 351, 495
- Sievers, A. W., Reuter, H.-P., Haslam, C. G. T., Kreysa, E., & Lemke, R. *A&A*, 281, 681
- Smith, J. 1982, *ApJ*, 261, 463
- Sodroski, T. J., et al. 1994, *ApJ*, 428, 638
- Stark, A. A., Davidson, J. A., Harper, D. A., Pernic, R., Loewenstein, R., Platt, S., Engargiola, G., & Casey, S. 1989, *ApJ*, 337, 650
- Stickel, M., et al. 2000, *A&A*, 359, 865
- Young, J. S., et al. 1995, *ApJS*, 98, 219

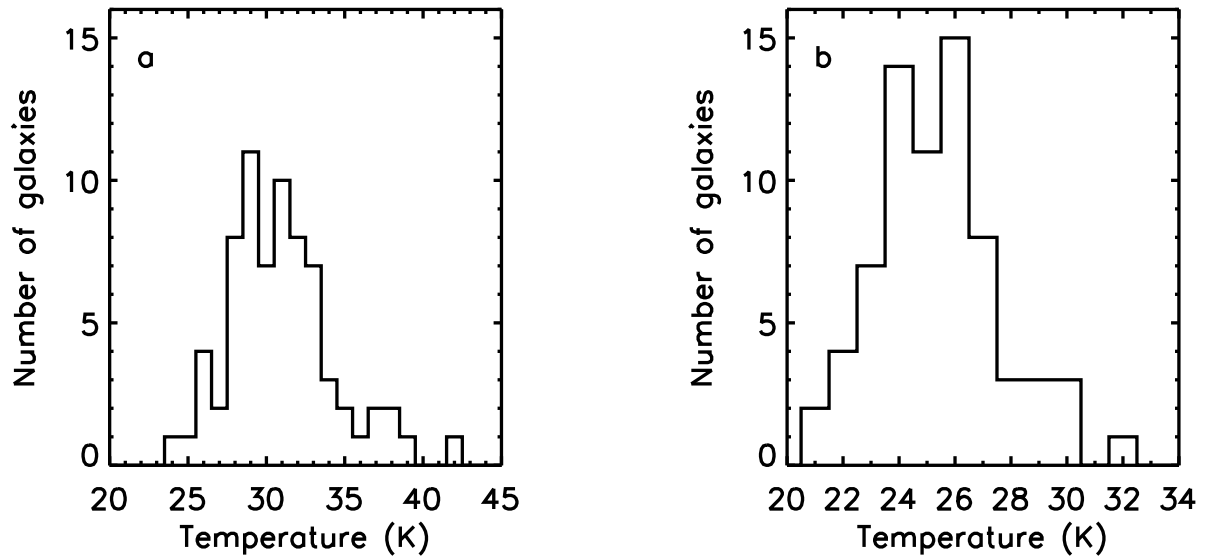


Fig. 1.— Histograms of the temperatures with (a) λ^{-1} and (b) λ^{-2} emissivities, as determined from the 60 - 180 μm data.

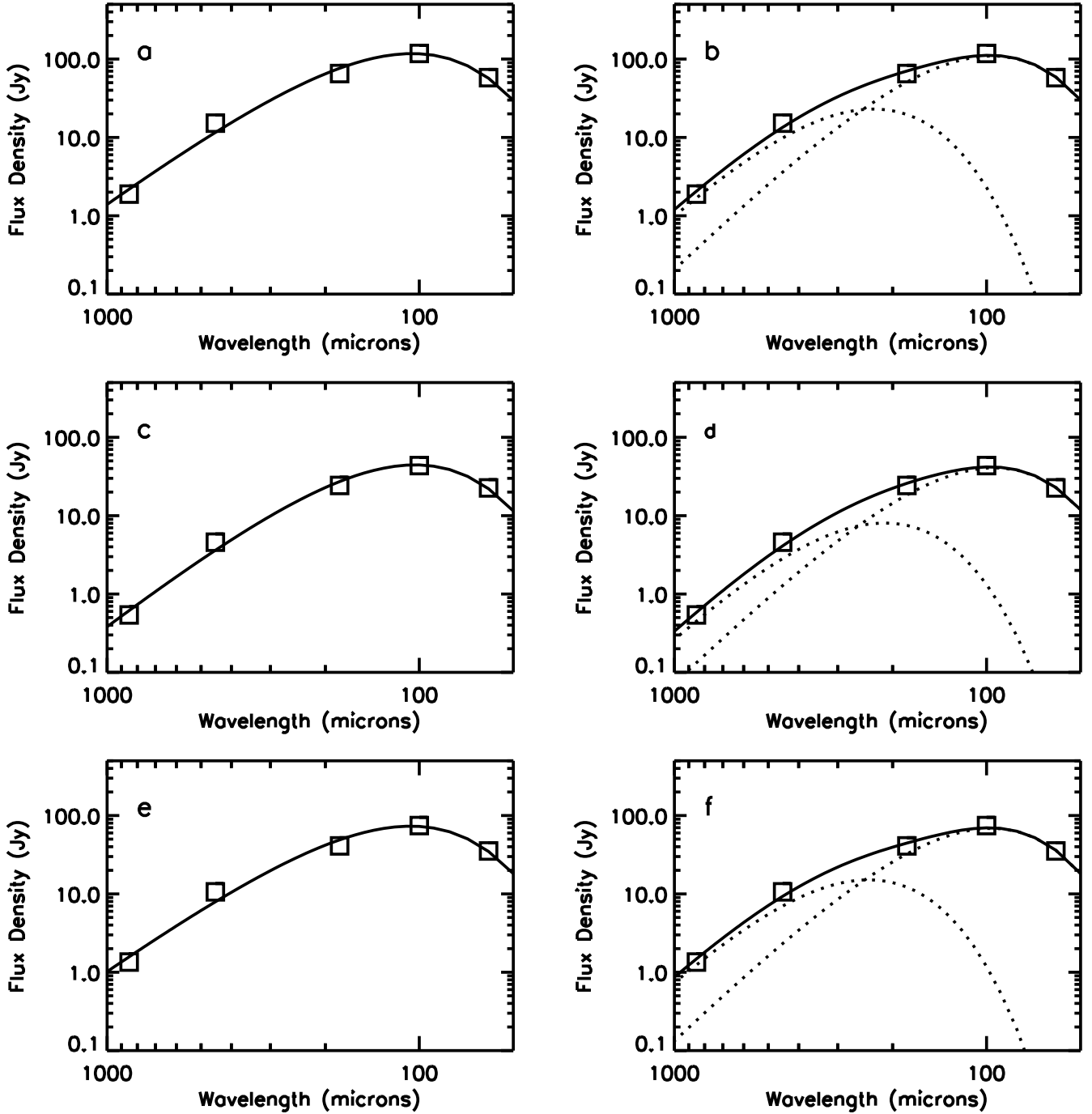


Fig. 2.— The (a & b) global, (c & d) nuclear, and (e & f) disk spectral energy distributions for NGC 4631. The measured data are represented by squares, and the errors for the data are less than the size of the squares. Parts a, c, and e show the best fitting blackbodies with $\lambda^{-\beta}$ emissivities (with β variable). Parts b, d, and f show the best fitting two blackbody components with λ^{-2} emissivities, with the dotted lines represent the individual blackbody components. This format also applies to Figures 3 - 9, although only the global spectral energy distributions are shown in those cases.

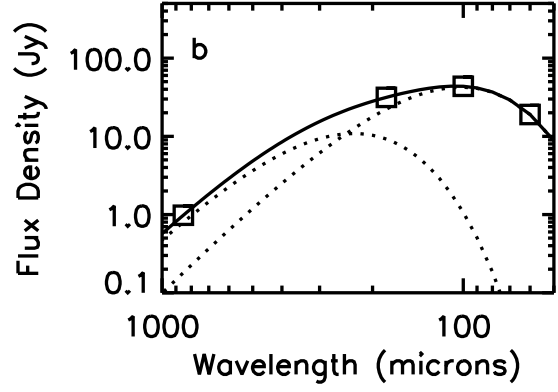
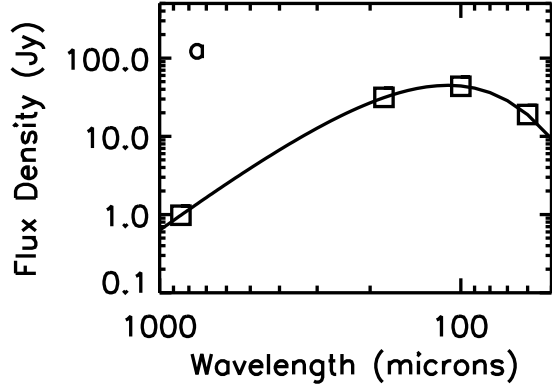


Fig. 3.— The global spectral energy distribution for NGC 4088.

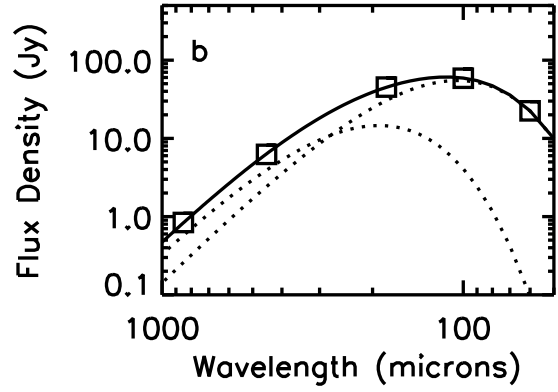
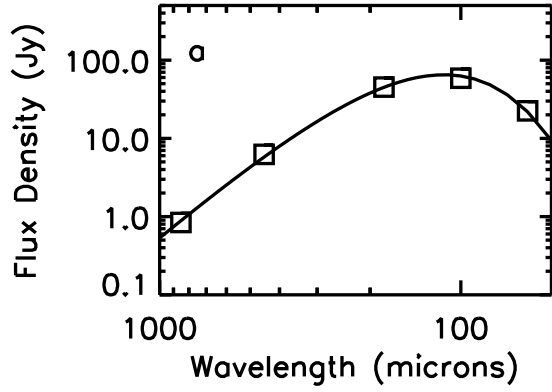


Fig. 4.— The global spectral energy distribution for NGC 4414.

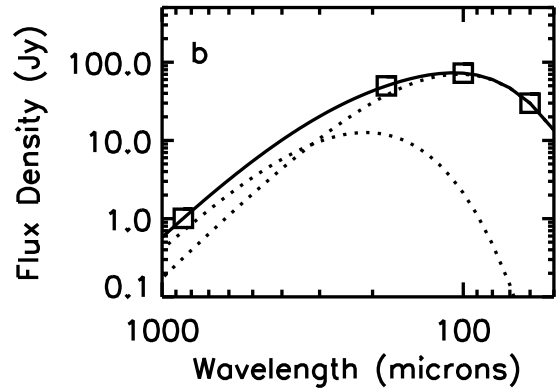
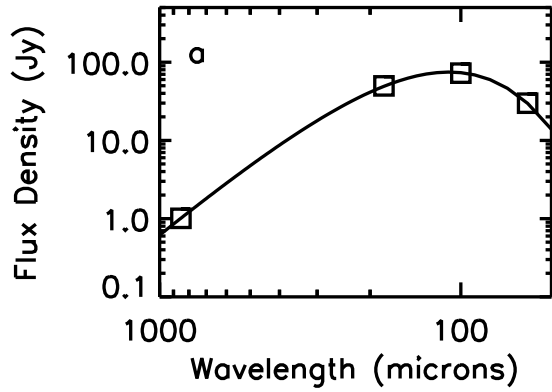


Fig. 5.— The global spectral energy distribution for NGC 4826.

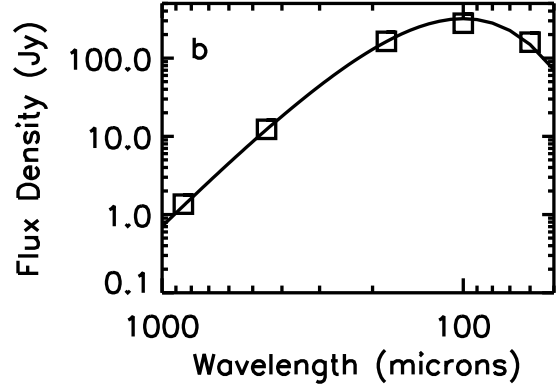
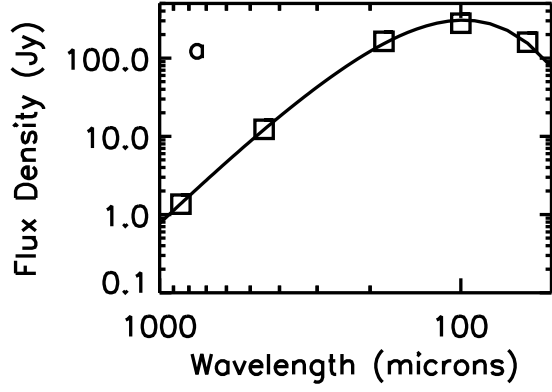


Fig. 6.— The global spectral energy distribution for NGC 5236.

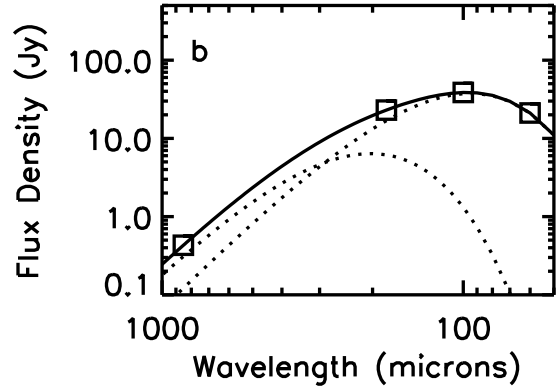
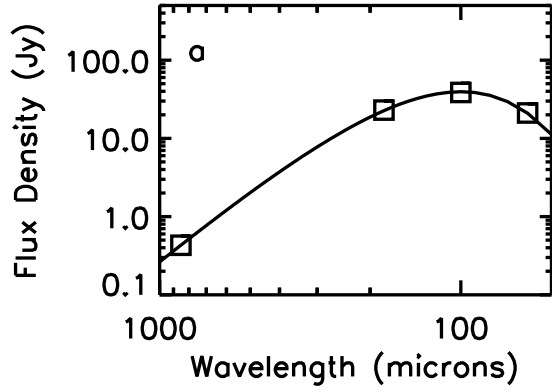


Fig. 7.— The global spectral energy distribution for NGC 5713.

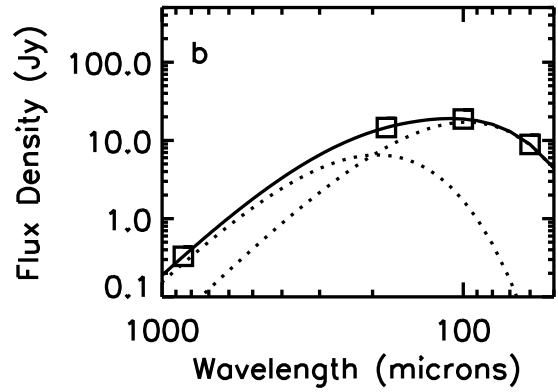
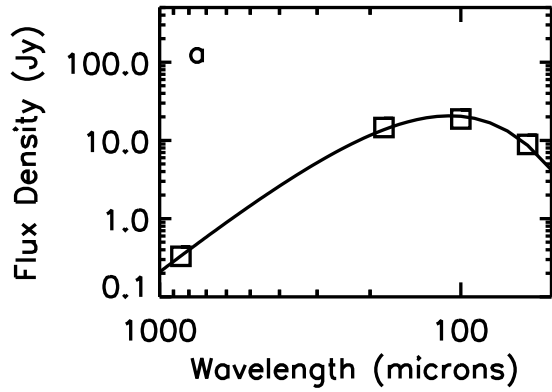


Fig. 8.— The global spectral energy distribution for NGC 5792.

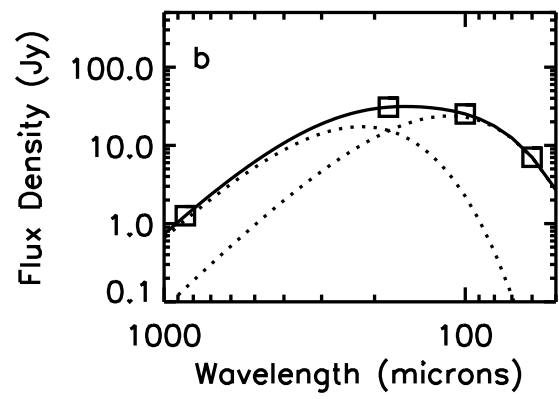
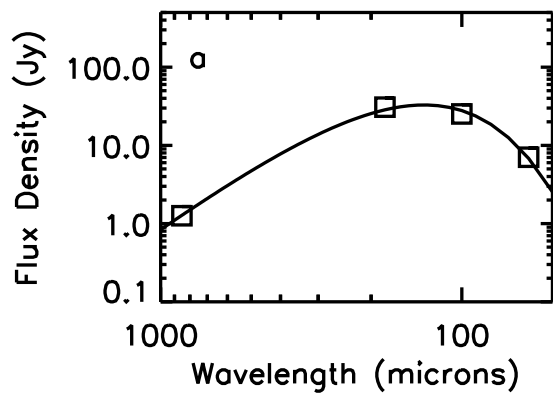


Fig. 9.— The global spectral energy distribution for NGC 5907.

TABLE 1
SUBMILLIMETER FLUX DENSITY MEASUREMENTS

Galaxy	450 μm Flux Density (Jy)		850 μm Flux Density (Jy)		$\log \log D_{25}^{\text{a}}$	Data Source
	45 arcsec	135 arcsec	45 arcsec	135 arcsec		
NGC 4088	0.26 ± 0.03	0.98 ± 0.10	1.76	Observation
NGC 4414	2.8 ± 0.3	7.3 ± 0.7	0.36 ± 0.04	0.84 ± 0.08	1.56	Archive
NGC 4631	4.8 ± 0.5	$18. \pm 0.2$	0.54 ± 0.05	1.89 ± 0.19	2.19	Archive
NGC 4826	0.63 ± 0.06	1.01 ± 0.10	2.00	Observation
NGC 5236	5.5 ± 0.5	9.7 ± 0.9	0.82 ± 0.08	1.36 ± 0.14	2.11	Archive
NGC 5713	0.26 ± 0.03	0.43 ± 0.04	1.44	Archive
NGC 5792	0.18 ± 0.02	0.33 ± 0.03	1.84	Archive
NGC 5907	0.43 ± 0.04	1.26 ± 0.13	2.10	Archive

^aThe optical diameter parameter defined in de Vaucouleurs et al. (1991).

TABLE 2
TEMPERATURES FROM FAR-INFRARED SPECTRAL ENERGY DISTRIBUTIONS

Galaxy	Temperature (K) ^a	
	λ^{-1} emissivity	λ^{-2} emissivity
NGC 55	26	22
NGC 289	31	25
NGC 1512	31	26
NGC 3359	32	26
NGC 3556	31	26
NGC 3898	30	25
NGC 4062	28	23
NGC 4088	31	25
NGC 4096	29	24
NGC 4100	33	26
NGC 4136	30	25
NGC 4157	29	24
NGC 4203	32	26
NGC 4236	32	26
NGC 4244	27	23
NGC 4274	29	24
NGC 4314	34	28
NGC 4395	26	22
NGC 4414	31	25
NGC 4448	30	25
NGC 4559	29	24
NGC 4605	32	26
NGC 4618	30	25
NGC 4631	34	27
NGC 4710	33	27
NGC 4725	24	21
NGC 4826	33	27
NGC 4984	39	30
NGC 5033	30	25
NGC 5054	31	26
NGC 5055	28	24
NGC 5087	38	30
NGC 5101	28	24
NGC 5102	29	24
NGC 5112	29	24
NGC 5170	28	24
NGC 5204	33	27
NGC 5236	36	29
NGC 5247	29	24
NGC 5300	29	24
NGC 5334	28	23
NGC 5364	26	22
NGC 5371	28	23
NGC 5457	27	23
NGC 5474	32	26
NGC 5556	33	27

TABLE 2—*Continued*

Galaxy	Temperature (K) ^a	
	λ^{-1} emissivity	λ^{-2} emissivity
NGC 5566	29	24
NGC 5584	32	26
NGC 5585	33	27
NGC 5669	29	24
NGC 5676	31	26
NGC 5701	31	25
NGC 5713	37	29
NGC 5746	28	23
NGC 5792	33	27
NGC 5838	42	32
NGC 5846	37	29
NGC 5850	30	25
NGC 5866	32	26
NGC 5907	26	22
NGC 5985	28	23
NGC 6015	29	24
NGC 6215	35	28
NGC 6217	35	28
NGC 6221	34	27
NGC 6300	31	26
NGC 6340	38	30
NGC 6503	30	25
NGC 6643	31	26
NGC 6744	25	21
NGC 6753	32	26

^aErrors on the temperature measurements are 2 K.

TABLE 3
DEPENDENCE OF FAR-INFRARED DUST TEMPERATURES ON MORPHOLOGICAL TYPE

Morphological Type	Number	Mean Temperatures (K) with λ^{-1} Emissivity	Mean Temperatures (K) with λ^{-2} Emissivity
All	71	30.9 ± 0.4	25.3 ± 0.3
E - S0/a	11	34.5 ± 1.4	27.5 ± 0.8
Sa - Sab	8	30.0 ± 1.1	25.0 ± 0.8
Sb - Sbc	19	30.3 ± 0.7	24.9 ± 0.5
Sc - Scd	25	30.2 ± 0.5	24.9 ± 0.3
Sd - Irr	8	30.9 ± 1.1	25.4 ± 0.8

TABLE 4
RESULTS OF DECONVOLUTION ANALYSIS ON 180 μM DATA

Galaxy	Measured 180 μm Flux Densities (180'') (Jy)	Deconvolved 180 μm Flux Densities (Jy)			
		in Components		in Set Apertures	
		Central	Extended (135'')	(45'')	(135'')
NGC 4088	46.2	8.4	23.	11.	31.
NGC 4414	54.5	22.	23.	25.	45.
NGC 4631	93.9	19.	46.	24.	65.
NGC 4826	51.8	18.	34.	34.	50.
NGC 5236	192.	90.	77.	99.	170.
NGC 5713	22.3	16.	7.	17.	23.
NGC 5792	15.9	8.7	6.0	9.3	15.
NGC 5907	44.1	9.1	22.	12.	31.

TABLE 5
TEMPERATURES WITH λ^{-1} EMISSIVITY

Galaxy	Global		Nuclear		Disk	
	Temp. (K) ^a	Reduced χ^2	Temp. (K) ^a	Reduced χ^2	Temp. (K) ^a	Reduced χ^2
NGC 4088	33.	0.014	35.	0.44	32.	0.17
NGC 4414	34.	3.0	35.	0.95	33.	12.
NGC 4631	35.	3.4	37.	3.5	34.	3.7
NGC 4826	35.	2.0	36.	2.2	32.	2.5
NGC 5236	45.	10.	48.	7.0	41.	18.
NGC 5713	39.	1.6	41.	2.9	34.	0.64
NGC 5792	35.	0.79	37.	1.4	30.	1.26
NGC 5907	27.	0.33	28.	0.46	27.	0.26

^aErrors on the temperature measurements are 2 K.

TABLE 6
TEMPERATURES WITH $\lambda^{-\beta}$ EMISSIVITY

Galaxy	Global			Nuclear			Disk		
	Temp. (K) ^a	β	Reduced χ^2	Temp. (K) ^a	β	Reduced χ^2	Temp. (K) ^a	β	Reduced χ^2
NGC 4088	34.	1.0	0.0055	33.	1.1	0.11	34.	0.9	0.0030
NGC 4414	29.	1.4	0.52	31.	1.3	0.66	26.	1.7	5.4
NGC 4631	35.	1.0	5.1	34.	1.2	3.8	35.	0.9	5.9
NGC 4826	31.	1.3	0.011	32.	1.3	0.11	28.	1.4	0.20
NGC 5236	30.	1.9	0.19	33.	1.7	0.80	26.	2.1	0.69
NGC 5713	34.	1.3	0.022	35.	1.4	0.15	31.	1.2	0.32
NGC 5792	32.	1.2	0.28	34.	1.2	0.82	27.	1.3	0.17
NGC 5907	28.	0.9	0.45	29.	0.9	0.83	28.	0.9	0.28

^aErrors on the temperature measurements are 2 K.

TABLE 7
TEMPERATURES WITH λ^{-2} EMISSIVITY

Galaxy	Global		Nuclear		Disk	
	Temp. (K) ^a	Reduced χ^2	Temp. (K) ^a	Reduced χ^2	Temp. (K) ^a	Reduced χ^2
NGC 4088	13. & 29.	...	14. & 30.	...	12. & 28.	...
NGC 4414	15. & 28.	0.031	7. & 27.	0.70	18. & 28.	6.1
NGC 4631	12. & 30.	2.5	14. & 31.	1.9	12. & 30.	2.9
NGC 4826	14. & 28.	...	15. & 30.	...	5. & 25.	...
NGC 5236	29.	0.29	30.	1.6	27.	0.78
NGC 5713	14. & 31.	...	16. & 33.	...	6. & 27.	...
NGC 5792	15. & 30.	...	17. & 34.	...	9. & 24.	...
NGC 5907	13. & 26.	...	14. & 27.	...	13. & 25.	...

^aErrors on the temperature measurements are 2 K.

TABLE 8
GLOBAL DUST MASSES AND GAS TO DUST RATIOS

Galaxy	Dust Masses (M_{\odot})			Molecular Gas Masses(M_{\odot})	Gas / Dust Ratios		
	λ^{-1} emissivity	λ^{-2} emissivity	$\lambda^{-\beta}$ emissivity		λ^{-1} emissivity	λ^{-2} emissivity	$\lambda^{-\beta}$ emissivity
NGC 4088	4.8×10^6	5.7×10^7	4.6×10^6	1.5×10^9	310.	26.	330.
NGC 4414	1.3×10^6	1.2×10^7	2.6×10^6	1.5×10^9	1200.	130.	580.
NGC 4631	1.4×10^6	2.1×10^7	1.4×10^6	4.4×10^8	310.	21.	310.
NGC 4826	2.7×10^5	2.7×10^6	4.5×10^5	1.8×10^8	670.	67.	400.
NGC 5236	3.5×10^5	2.0×10^6	1.7×10^6	9.5×10^8	2700.	480.	560.
NGC 5713	5.5×10^6	6.5×10^7	9.3×10^6	3.0×10^9	550.	46.	320.
NGC 5907	6.2×10^6	5.9×10^7	5.2×10^6	7.8×10^8	130.	13.	150.